LIMNOLOGY and OCEANOGRAPHY

ASLO

Limnol. Oceanogr. 9999, 2023, 1–15

doi: 10.1002/lno.12476

The role of seasonal hypoxia and benthic boundary layer exchange on iron redox cycling on the Oregon shelf

Natalya Evans,[1] **Alexis E. Floback**,[1] **Justin Gaffney**,[1] **Peter J. Chace**,[2] **Zachary Luna**,[2] **Joël Knoery**,[3] **Clare E. Reimers**,[2] **James W. Moffett**[1*]

[1]Department of Biological Sciences, University of Southern California, Los Angeles, California, USA
[2]College of Earth, Ocean, and Atmospheric Sciences, Oregon State University, Corvallis, Oregon, USA
[3]Ifremer, Unité Contamination Chimique des Ecosystèmes Marins, Nantes, France

Abstract

Widespread hypoxia occurs seasonally across the Oregon continental shelf, and the duration, intensity, and frequency of hypoxic events have increased in recent years. In hypoxic regions, iron reduction can liberate dissolved Fe(II) from continental shelf sediments. Fe(II) was measured in the water column across the continental shelf and slope on the Oregon coast during summer 2022 using both a trace metal clean rosette and a high-resolution benthic gradient sampler. In the summer, Fe(II) concentrations were exceptionally high (40–60 nM) within bottom waters and ubiquitous across the Oregon shelf, reflecting the low oxygen condition (40–70 μM) at that time. The observed inverse correlation between Fe(II) and bottom water oxygen concentrations is in agreement with expectations based on previous work that demonstrates oxygen is a major determinant of benthic Fe fluxes. Rapid attenuation of Fe(II) from the benthic boundary layer (within 1 m of the seafloor) probably reflects efficient cross-shelf advection. One region, centered around Heceta Bank (~ 44°N) acts a hotspot for Fe release on the Oregon continental shelf, likely due to its semi-retentive nature and high percent mud content in sediment. The results suggest that hypoxia is an important determinant of the inventory of iron is Oregon shelf waters and thus ultimately controls the importance of continental margin-derived iron to the interior of the North Pacific Basin.

Iron (Fe) is a crucial element for biological processes and can limit primary productivity, especially in nutrient-rich ecosystems (Boyd and Ellwood 2010; Tagliabue et al. 2017). The continental margin acts as one of the primary sources of Fe to the interior basin (Lam and Bishop 2008), and the chemistry of iron influences its fate and transport. In the presence of oxygen, thermodynamically favored Fe(III) quickly precipitates to form Fe (oxy)hydroxides that sink out of the water column. However, Fe(III) can be complexed by organic ligands, keeping that Fe dissolved and increasing its residence time in the water column (Vraspir and Butler 2009).

Under anoxic conditions, Fe(III) can be reduced to Fe(II) by microorganisms through a variety of mechanisms, including dissimilatory iron reduction and reduction by sulfide (Raiswell and Canfield 2012). Fe(II) is highly soluble and persists until it is re-oxidized to Fe(III). The reductive dissolution of iron within shelf sediments and its release into the overlying waters act as the first two steps of the shelf-to-basin iron shuttle (Canfield et al. 1996; Reed et al. 2016). The shelf-to-basin iron shuttle has been proposed as one of the primary mechanisms for Fe transport offshore from continental margins (Severmann et al. 2010).

Continental margins that intersect Oxygen Deficient Zones (ODZs) may represent especially important source regions for Fe. In ODZs, the dominant water column metabolisms reduce nitrogen compounds (Ulloa et al. 2012); however, iron reduction occurs in sediments intersected by ODZs, and mesoscale circulation features can transport Fe(II) beyond the shelf within a narrow density range that intersects the margin sediments (Vedamati et al. 2014; Bolster et al. 2018; Cutter et al. 2018). This off-shelf Fe(II) may precipitate to Fe(III),

*Correspondence: jmoffett@usc.edu

Additional Supporting Information may be found in the online version of this article.

Author Contribution Statement: N.E. carried out all of the iron(II) analyses, performed the computational work and data synthesis and co-wrote the manuscript. A.F. performed all the analyses for total dissolved iron and reviewed the manuscript. N.E., A.E., J.G., Z.L., and J.M. participated in the sample collection, processing, and storage. P.C. and Z.L. deployed the benthic sampler and retrieved samples. C.E. supervised P.C. and participated in data synthesis and interpretation. J.M. designed the project, supervised N.E., and revised the manuscript.

settle onto the continental slope, and be remobilized to form a deep plume of dissolved Fe(III) (Lam et al. 2020). These deep plumes have been observed in all three oceanic ODZs: the Eastern Tropical North Pacific (ETNP), Eastern Tropical South Pacific (ETSP), and the Arabian Sea (Thi Dieu Vu and Sohrin 2013; Resing et al. 2015; Bolster et al. 2022; Chinni and Singh 2022) as well as highly productive Oxygen Minimum Zones (Noble et al. 2012; Hatta et al. 2015), though their appearance is not predicted by classical geochemical models (Lam et al. 2020).

The observations of deep Fe plumes have prompted renewed interest in off-shelf Fe transport. Mechanistic and modeling studies have suggested the importance of nonreductive dissolution of iron (König et al. 2021) and its transport via colloids (Homoky et al. 2021). In coastal waters, both resuspension of iron particles (Johnson et al. 1999) as well as reductive dissolution have been identified as sources of iron (Severmann et al. 2010; Fuchsman et al. 2015). Benthic Fe fluxes have been parameterized as a function of both bottom water O_2 concentrations as well as carbon oxidation rate (Elrod et al. 2004; Severmann et al. 2010; Dale et al. 2015). A recent parameterization of Fe in a regional model for the United States west coast has shifted to using only the bottom water O_2 concentration (Deutsch et al. 2021). Studies of the reductive dissolution of sedimentary Fe have been performed on the United States west coast using benthic chambers (Homoky et al. 2016). These studies provide excellent data on benthic fluxes but rarely link these benthic flux measurements to water column Fe concentrations.

Other sources of Fe to the ocean include dust deposition and river inputs. Dust deposition is a major source of Fe to the open ocean; however, dust reaching the Pacific Ocean originates primarily from Asia (Jickells et al. 2005) and is less significant in Oregon coastal waters. Rivers are also a source of Fe to the ocean, and off the coast of Oregon, the Columbia River provides significant inputs (Buck et al. 2007; Berger et al. 2008; Bruland et al. 2008). A number of rivers smaller than the Columbia River including the Rogue, Umpqua, and Nehalem rivers also act as sources of particulate Fe to Oregon coastal waters (Wetz et al. 2006). Studies further south on the California coast have surmised that sediments on the continental margin act as the primary source of Fe to coastal waters (Johnson et al. 1999). Coastal Oregon bottom waters contain high concentrations of both Fe(III) and Fe(II) under hypoxic conditions in summer (Lohan and Bruland 2008).

Summer hypoxia events have been becoming longer and more pronounced over the 21st century (Pierce et al. 2012). A combination of low O_2 waters upwelling onto the continental shelf, retention of these waters, and local respiration within the water column and at the seafloor leads to hypoxic conditions (Siedlecki et al. 2012). Shelf width significantly influences sediment accumulation rates, grain size, and both organic carbon and particulate iron enrichment in coastal sediments due to riverine inputs, along shore transport and the influences of submarine rock outcrops off Oregon (Kulm et al. 1975). More material is transported during peak winter river discharges and when wave energy is elevated, but during summer, fine sediments settle onto the shelf and undergo extensive bioturbation as well as diagenetic remineralization (Kulm et al. 1975; Chase et al. 2007).

Oregon provides an excellent study site for the Fe cycle not only because of the previous research there but also its hydrographic features. Along the Oregon coast, the poleward flowing California Undercurrent interacts with seafloor topography along the shelf-slope break. This interaction can lead to the formation of eddies at the depth horizon of the shelf-slope break (Molemaker et al. 2015), and these mesoscale features can move materials, including Fe, off the continental margin. The stronger the poleward current, the more pronounced the eddies (Frenger et al. 2018), but seafloor topography, particularly banks, ridges and canyons can enhance eddy formation. Such eddies are important for Fe transport because their generation involves instability of bottom boundary layer waters that have been in contact with sediments, usually with low O_2 concentrations. Eddy-driven transport is highly active along the Oregon coast (Damien et al. 2023).

The Oregon coast is near the northernmost extent of the California Undercurrent, which together with upwelling supplies nutrient-rich but O_2-poor water to the shelf (Thomson and Krassovski 2010). As the undercurrent moves along the continental margin, elevated remineralization rates continue to lower the oxygen within these waters (Meinvielle and Johnson 2013; Evans et al. 2020), such that these waters have especially low O_2 once they reach Oregon. Anoxia was observed off the Oregon coast in 2006—a year of exceptionally severe hypoxia across the shelf (Chan et al. 2008).

The switch from hypoxic to anoxic respiration has major ramifications for a highly productive ecosystem such as the northern California Current System. In the summer of 2002, shoaling of hypoxic waters onto the shallow shelf damaged Oregon's Dungeness crab population, a fishery worth $50 million annually (Chan et al. 2019). This change will also significantly magnify the flux of Fe from this continental margin into the Northeast Pacific Ocean, where productivity is limited by Fe (Moore et al. 2013). Understanding the current processes controlling the continental margin Fe source, such as its redox speciation, accumulation, and export, may improve our ability to predict future ecosystem conditions in this region.

Previous work off the Oregon Coast has demonstrated the important relationship between bottom water oxygen and benthic Fe fluxes using benthic chambers (Severmann et al. 2010). In this study, our objectives were twofold. First, we wanted to determine if bottom water oxygen was also an important determinant of dissolved iron inventory in the overlying water column, particularly in the benthic boundary layer. Second, we wanted to determine if the relationship between bottom water oxygen and dissolved Fe in the water column could be explained by the persistence of significant

concentrations of Fe(II) within the benthic boundary layer and the overlying water column. We focused on specific locations that were studied in Severmann et al. (2010) as well as other regions characterized by persistent summer hypoxia.

Materials and methods

Sampling description

Water samples from the Oregon continental margin were collected from the R/V *Oceanus* during cruise OC2107A, which was conducted from July to August 2021 (Fig. 1) as part of the Iron Transport Shuttle Program. Stations 32 and 33 sampled the water column at the same locations as the Umpqua River-influenced stations studied by Severmann et al. (2010), and stations 25–29 were on the well-characterized Newport Hydrographic Line (Adams et al. 2016). Station 20 was located at the Columbia River depocenter (Nittrouer et al. 1979), whereas station 34 was located at the Umpqua River depocenter.

A standard Seabird CTD-rosette equipped with a SBE43 sensor and 10 liter Niskin bottles was used to measure dissolved oxygen profiles and retrieve samples for nutrient analyses. Oxygen measurements consist of data measured during upcasts and averaged every meter. Data were smoothed using moving averages with a 5 m bin. Iron samples were collected primarily using 5 liter Teflon-coated external spring Niskin-type bottles (Ocean Test Equipment) with a stand-alone trace metal clean rosette (Sea-Bird Electronics) that was controlled by an autofire module that tripped the bottles during upcasts. This rosette was deployed with a dedicated MASH 2K winch spooled with a non-contaminating hydrowire (Amsteel). Closed bottles were hand-carried to a clean lab space constructed from polyethylene plastic sheeting with high efficiency particulate air (HEPA) filters to prevent contamination. All plastic used to handle trace metal samples was cleaned prior to use with a 1-d soak in Citranox then a week soak in 10% hydrochloric acid. Plastic used to handle Fe(II) was also soaked in milliQ water for 2 d after acid washing to remove any residual acid.

The trace metal clean rosette lacked an altimeter and therefore could not sample close to the seafloor, so a few near-bottom Fe(II) samples were collected using the ship's traditional CTD rosette Niskin bottles in high Fe(II) bottom waters. When collecting Fe(II) samples from the CTD Niskins, we overlapped some sampled depths with the trace metal clean

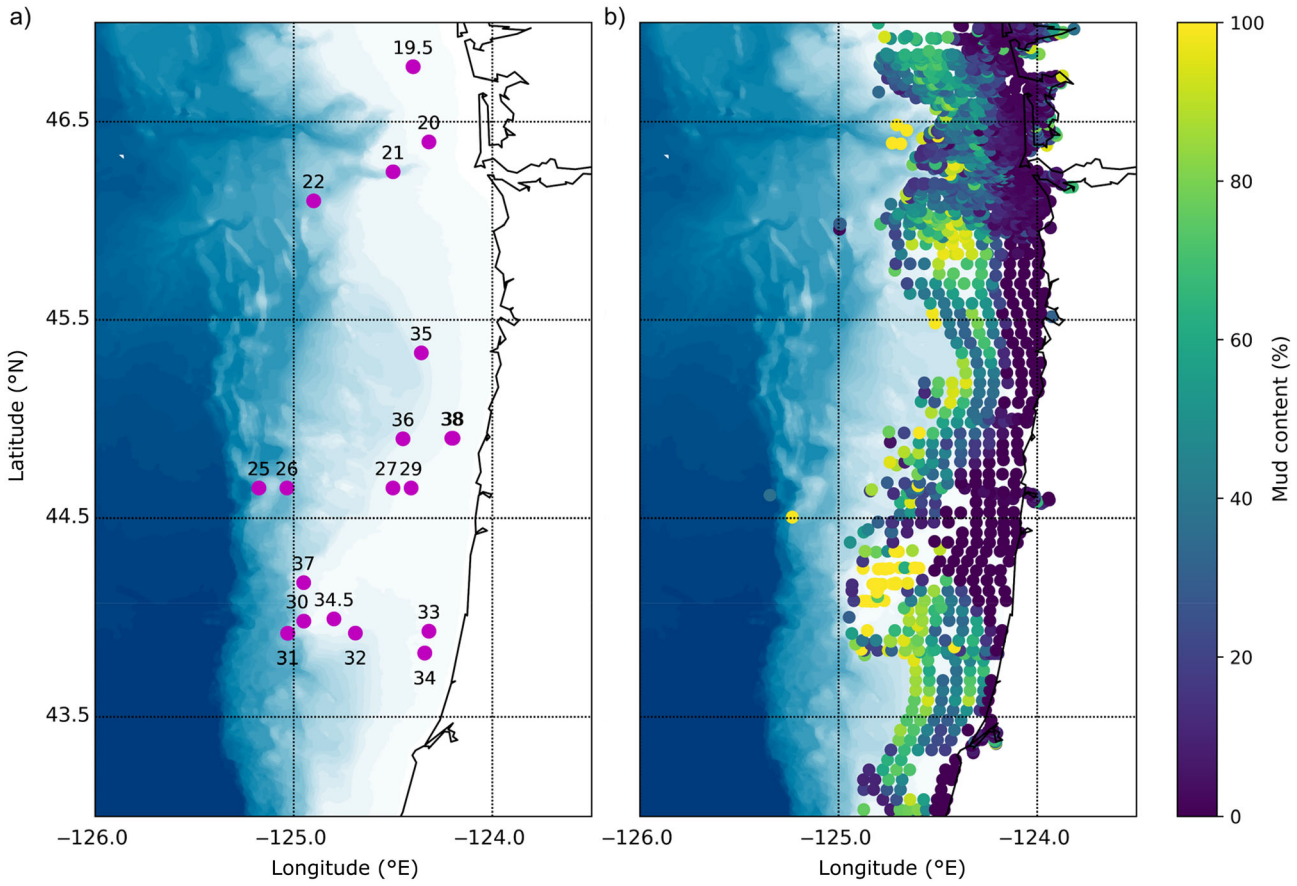

Fig. 1. (**a**) Sampling map for OC2107A stations with bathymetry shaded in blue. A solid black line indicates the coastline. (**b**) Same coastline and bathymetry, but the measured sediment mud content (% silt and clay fraction) from the usSEABED database is presented.

depth profile to enable comparison between these two methods. At Stas. 19.5 and 33, a benthic boundary gradient sampler mounted on an aluminum tripod frame was deployed using the ship's 9/16″ trawl wire to collect samples within 1.5 m of the seafloor. This lander held a syringe sampler named "Susane," designed to draw up to 18 samples simultaneously from known heights (Knoery et al. 2019) and was triggered using a timed burn-wire. Next, 60 mL polypropylene/polyethylene sampling syringes (Air-Tite, VWR) were cleaned with isopropyl alcohol and 0.5 M hydrochloric acid and flushed with N_2-purged water and kept in a continuously purging bath for at least 6 hr prior to sampling to reduce oxygen contamination. While the syringe sampler is designed to flush sample lines using in situ fluid prior to drawing samples, all sampling lines and syringes were further flushed with N_2-purged deionized water to limit diffusion from walls of sample lines and syringes.

Chemical measurements

Fe samples were filtered using Pall Gelman Supor 0.45 μm polyethersulfone filters with either Millipore Swinnex polypropylene 25 mm filter holders or Advantec-MFS type PP47 47-mm polypropylene inline filter holders, as recommended by the GEOTRACES Cookbook version 3.0 (Cutter et al. 2018). N_2 gas was used to pressurize the Niskin bottles during filtration. Filtered fractions for Fe(II) measurement were transferred to a syringe using a three-way Luer-lock adaptor to prevent the introduction of air, stored in an ice bath to lower oxidation rates while they were in cue to be measured, then measured within 2 hr. No samples were shaken. We recorded the times between collection and measurement to correct for oxidative losses of Fe(II). Fe(II) was measured via chemiluminescence with luminol, consisting of a continuous 2 mL min^{-1} flow of sample and luminol solution at a 1 : 1 ratio into a FeLume system (Waterville Analytical) comprised of a quartz flow cell with a Hamamatsu HC135 photon counter via a peristaltic pump. The signal value for each sample was determined as the mean of the signal for 30 s ($n = 50$), once the signal reached steady state. The order of sample measurement was randomized to prevent systematic error due to sample oxidation.

Each sample was also treated with diethylenetriamine pentaacetate (DTPA), a selective Fe(II) chelator used as a masking ligand. The DTPA-treated samples, with a final concentration of 0.5 mM DTPA, serve to correct for a well-documented interference that arises from nonmetals (Bolster et al. 2018). DTPA chelates Fe(II) and oxidizes it to Fe(III) virtually instantaneously. Any residual chemiluminescent signal can be attributed to other redox active species. DTPA-treated samples were processed with the exact same analytical train as untreated Fe(II) samples.

Fe(II) calibration was performed each time the system was powered on and calibration curves consisted of six or more concentrations within the appropriate working range of the measured Fe(II) (Supporting Information Fig. S1). These concentrations were created by spiking a seawater solution that aged for at least 24 h in an amber bottle with an appropriate volume of 1 μM Fe(II) working stock in milliQ water. This working stock was created fresh before calibration from a 0.01 M Fe(II) standard solution at pH 2, prepared monthly by dissolving Optima grade hydrochloric acid (Fisher) and ammonium ferrous sulfate (Fluka) in milliQ water. Luminol solutions were prepared first using a stock solution with 0.796 g of sodium luminol (Sigma), 250 mL of Optima grade ammonium hydroxide (Fisher), approximately 45 mL of Optima grade hydrochloric acid (Fisher), and milliQ water. The working luminol reagent was produced by diluting this stock to one-fourth its starting concentration, then heating it at 50 °C for 9–12 hr. The DTPA solution was created by diluting DTPA (Millipore-Sigma) with sodium hydroxide (Aldrich, trace metal basis) in milliQ water for a final concentration of 50 mM DTPA and 200 mM NaOH. Additional details of this method including reagent preparation, instrumental settings, and procedures have been previously reported (Bolster et al. 2018).

Bolster et al. (2018) added MOPS (3-[*N*-morpholino]propanesulfonic acid) upon sampling to buffer the pH to 7.0 to slow oxidation of Fe(II) between sampling and analysis. This was not possible with Susane. Fortunately, the oxidation rate of Fe(II) under the prevailing pH and temperature near the seafloor were slow enough for the Fe(II) concentration at the time of sampling by extrapolation (*see* below). The pH was measured on most samples using an Oakton pH 150 portable meter kit.

Total dissolved Fe samples were collected into 500-mL low-density polyethylene (LDPE) bottles. Within 1 month of collection, these samples were acidified to a pH of approximately 1.7 by adding 1 mL of hydrochloric acid (Optima, Fisher Scientific) per 500 mL of seawater. Samples were analyzed after 6–12 months of storage. Samples were prepared in triplicate using the seaFAST-pico (Elemental Scientific) offline method, where 10 mL of acidified sample was added to a Nobias resin chelation column then eluted with ultrapure, distilled 5% nitric acid (Optima, Fisher Scientific) for a final volume of 0.5 mL. This method is similar to the method described by Jackson et al. (2018) and Rapp et al. (2017). Fe concentrations were quantified with a Finnegan Element 2 (Thermo Scientific) Inductively Coupled Plasma-Mass Spectrometer and Apex desolvation system in medium resolution. A 1-ppb indium eluent is used during sample preparation as an internal standard to correct for instrument drift. Instrument optimization and tuning are performed daily with a 1-ppb indium and uranium tuning solution. Procedural blanks were prepared in triplicate from pH 1.7 hydrochloric acid to correct for contamination during acidification of samples. Sample concentration of Fe was determined via isotopic dilution method (Milne et al. 2010), in which acidified samples were spiked with a multielement standard, including ^{57}Fe, enriching it over the natural isotopic abundances.

Oxygen concentrations from the benthic boundary gradient sampler were measured less than an hour from recovery using a Presens fast response Flow-Through Cell FTCH-PSt1 Microsensor interfaced with a Presens TX-3 meter in a flow cell fitted to the sampling syringe outlets. Between each O_2 measurement, brief flushes of nitrogen gas were also used to check for calibration shifts and remove contamination between samples. The order of sample measurement was randomized to reduce the influence of any contamination post-recovery.

Computational methods

MATLAB R2018B (The MathWorks, Inc. 2018) was used to read in and average signal values for Fe(II) measurement. The calibration curve for Fe(II) using this method follows a second-order polynomial as described in Bolster et al. (2018), so the "nllsqr" function (Glover et al. 2011) was used to fit these data using an equation with the form $a_1x^2 + a_2x + a_3$. An example calibration is included in Supporting Information Fig. S1. Sample concentrations were calculated by first subtracting the DTPA signal then applying the "vpasolve" command with the given calibration curve. The uncertainty in measured Fe(II) concentrations was calculated using the standard error of the signal at steady state ($n = 50$). For Fe(II) samples measured in duplicate, the uncertainty consists of this standard error and the standard deviation of the two measurements added in quadrature.

Previous measurements of Fe(II) by our group were in oxygen-free waters and oxidation rates were so slow that it is a reasonable assumption that the Fe(II) concentration at the time of analysis was equal to the Fe(II) concentration at the time of collection (i.e., sample bottle or syringe closure) designated $Fe(II)_{t=0}$. In this study, where samples were hypoxic but not anoxic, oxidation of Fe(II) by molecular oxygen occurred between sampling and analysis. Therefore, we had to generate an estimate of the rate of oxidation in order to estimate $Fe(II)_{t=0}$.

The rate law for Fe(II) oxidation is provided in Eq. 1. We followed the derivation in Gonzales-Santana et al. (2021) for Fe(II) oxidation rates, using the pseudo-first-order assumption for Eqs. 2 and 3.

$$\frac{d\mathrm{Fe(II)}}{dt} = -k[\mathrm{O_2}][\mathrm{Fe(II)}] \quad (1)$$

$$k' = -k[\mathrm{O_2}]_{\mathrm{sat}} \quad (2)$$

$$\frac{d\mathrm{Fe(II)}}{dt} = -k'[\mathrm{Fe(II)}] \quad (3)$$

Gonzalez-Santana et al. (2021) use the expression in Eq. 4 for the empirically derived rate constant for Fe(II) oxidation based on data in Santana-Casiano et al. (2005)

$$\log(k') = 35.627 - 6.7109(\mathrm{pH}) + 0.5342(\mathrm{pH})^2 - \frac{5362.6}{T} - 0.04406(S)^{0.5} - 0.002847(S) \quad (4)$$

However, the values of k' determined from this equation were for saturated oxygen concentrations at these temperature, salinity, and pH conditions (Santana-Casiano et al. 2005). Our samples were significantly undersaturated with respect to oxygen. Since the rate of oxidation is proportional to the oxygen concentration (Eq. 1), we needed to modify the predicted oxidation rate by the following expressions:

$$\frac{d\mathrm{Fe(II)}}{dt} = -k'\left(\frac{[\mathrm{O_2}]}{[\mathrm{O_2}]_{\mathrm{sat}}}\right)[\mathrm{Fe(II)}] \quad (5)$$

$$\tau_{\frac{1}{2}} = \frac{\ln(2)}{k'\left([\mathrm{O_2}]/[\mathrm{O_2^{sat}}]\right)} \quad (6)$$

We calculated the O_2 saturation using TEOS-10.

Measured pH values were used to calculate the Fe(II) oxidation rates. We also compared the calculated oxidation rate with an experimentally determined rate and observed close agreement (Supporting Information Section S2, Fig. S2). Stas. 19.5 and 20 lacked pH measurements, as did benthic lander samples, so the pH for these samples was approximated using a correlation between pH and O_2. This pH approximation is described further in Supporting Information Section S3 and Fig. S3. Uncertainty in $Fe(II)_{t=0}$ concentrations was calculated by combining the uncertainty in the measured Fe(II) with the error in the measured pH. These calculations are specified explicitly in the Supporting Information, and the equation to calculate the half-life is included in Eq. 6.

Sediment properties were downloaded from the usSEABED database (https://www.usgs.gov/programs/cmhrp/science/usseabed), a unified, comprehensive database of seafloor properties in the US Exclusive Economic Zone. The US9_EXT data product was used for this study. Mud has a specific definition in the database, derived from grain size, silt, and clay content, that is described in its supporting documentation. The data product consists of discrete samples, so we interpolated the sediment mud content to our station locations to assess if water column Fe concentrations possessed any relationship to sediment texture. These sediment data were cleaned by removing any samples deeper than 500 m, west of −123.5°E, outside of 42–47°N, and missing mud percentage. Some samples within regions of interest were missing depth, so we first interpolated longitude and latitude to depth using the scatteredInterpolant command and the "natural" interpolation option in MATLAB R2018B. We interpolated the sediment mud content (the percent silt and clay fractions) using the same computational set up, but we included longitude, latitude, and depth to create the interpolation surface for sediment mud content. We set a constant uncertainty for the interpolated mud content using the mean of the residuals between the interpolated and the original mud values, which was 3.3%.

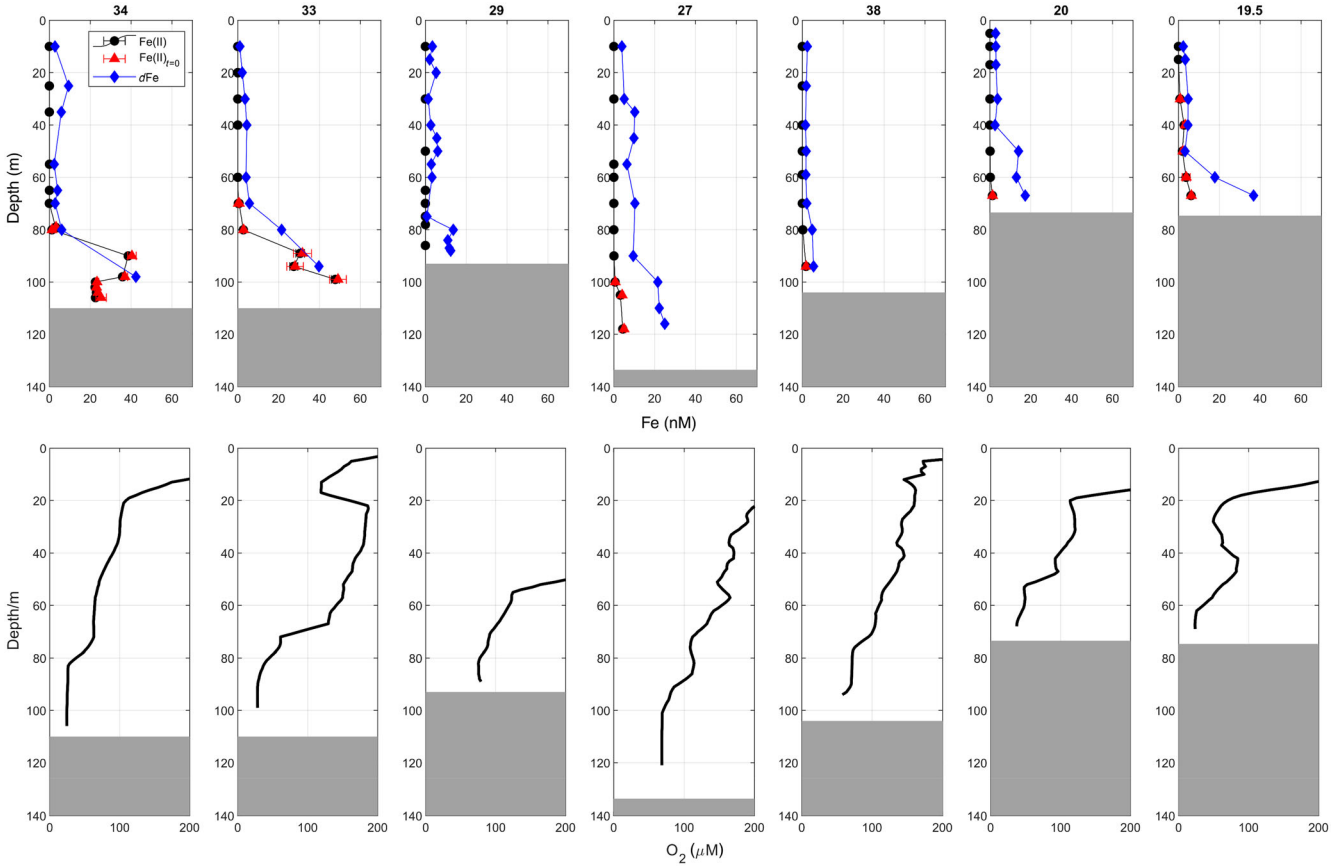

Fig. 2. Depth profiles of Fe(II), $Fe(II)_{t=0}$ (which is corrected for oxidation between sampling and measurement), dissolved Fe, and O_2 for selected shelf stations. The upper row displays the Fe data, whereas the bottom row depicts O_2. Station numbers are specified on the top of each Fe profile, and this station number applies to the O_2 profile below it. The gray region on the bottom of each profile indicates the depth of the seafloor, as estimated by the ship's echosounder while on station. Measured Fe(II) concentrations were so low at station 29 that $Fe(II)_{t=0}$ could not be calculated. pH measurements were not collected at stations 19.5 and 20, so $Fe(II)_{t=0}$ at these stations used estimated pH values.

Scatter and section plots were generated using MATLAB R2018B, and TEOS-10 calculations (McDougall and Barker 2011) were performed in MATLAB as well with the IBM ILOG CPLEX Optimization Studio V12.8.0 as an optimizer. Maps were plotted using Python 3.7.13 (Python Software Foundation 2022) in Spyder 5.1.5 (Raybaut 2009) with the Basemap package (Hunter 2007), and perceptually uniform colormaps were used to improve accessibility as well as scientific accuracy (Thyng et al. 2016; Biguri 2021). Bathymetry data were downloaded from the National Centers for Environmental Information 3 arc-second resolution coastal relief model (https://www.ngdc.noaa.gov/mgg/coastal/crm.html). Contour plots were interpolated first along each station using linear or nearest neighbor algorithms at high resolution, then interpolated across longitude linearly.

Results

Cross-shelf variability in iron

Dissolved Fe concentrations in continental margin bottom waters have been linked to many factors, such as oxygen concentration, carbon oxidation rate, shelf width, and sediment mud content. We analyzed Fe data at eight stations along the mid-shelf (depth < 150 m) to probe the roles of these different factors (Fig. 2). The depth profile features within these three groups: the Heceta Bank, Newport Hydrographic Line, and Columbia River, are more similar to each other than they are between groups. Heceta Bank stations exhibited only 25–30 μM O_2 in their bottom waters and they had the highest dissolved Fe and Fe(II) concentrations with 40–60 nM dissolved Fe and 22–58 nM Fe(II). The Columbia River stations had similarly low O_2, with 23 and 37 μM, but drastically different Fe profiles. At station 19.5, dissolved Fe was 37 nM, but Fe(II) was only 6.2 nM, whereas station 20 was lower in both categories. The Newport Hydrographic line stations had the highest O_2 during this sampling campaign, ranging from 68 to 76 μM, and the lowest Fe, with 5.5–25 nM dissolved Fe and 1.2–4.4 nM Fe(II).

Stations 27, 20, and 19.5 reveal elevated Fe near the bottom, like the ratio is Heceta Bank stations, but the Fe(II)/dissolved Fe ratio is significantly lower. Low Fe(II) relative to dissolved Fe suggests that while these waters may have a

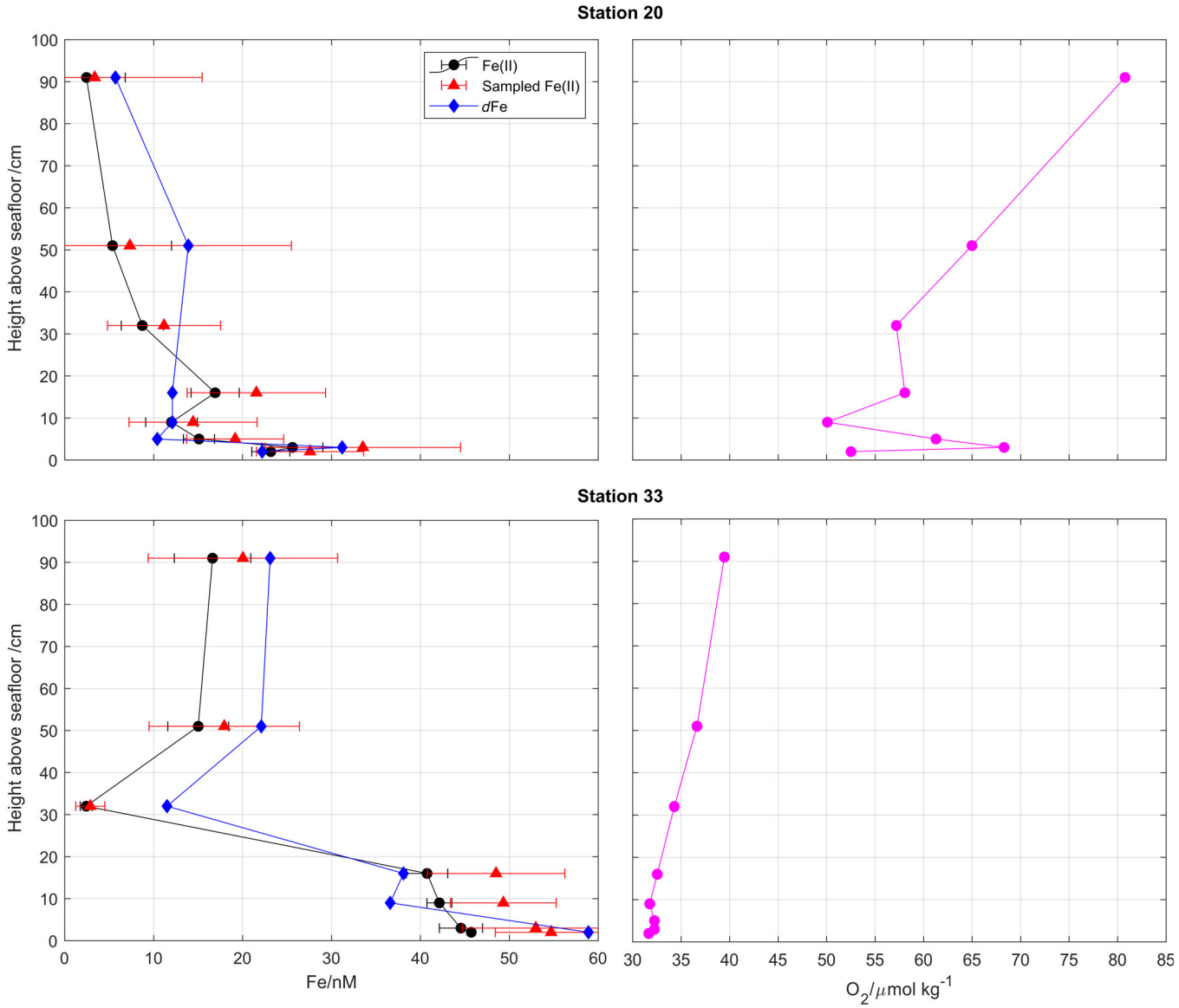

Fig. 3. Fe(II), $Fe(II)_{t=0}$, dissolved Fe, and O_2 profiles from two benthic lander deployments on the Oregon continental margin.

strong benthic source of Fe(II), oxidation occurred between release across the sediment water interface and our sampling. This interval in time and space probably reflects local physics, perhaps advection from elsewhere or slower vertical release from the seafloor than in waters overlying the Heceta Bank.

Benthic release of iron

We collected high resolution benthic boundary layer samples at stations 20 and 33, representing both the Columbia River and Heceta Bank regions. The near-sediment O_2 concentration at station 20 was twice that of station 33, and the resulting Fe(II) and dissolved Fe concentrations in the samples nearest the seafloor at station 20 were approximately half that of station 33. At both stations, the concentrations of Fe(II) and dissolved Fe were nearly equal near the seafloor, suggesting that Fe(II) was the dominant form of Fe. This evidence points to Fe being released from the sediments through reductive dissolution, which is expected based on the low oxygen concentrations measured at these locations. At several depths, we observed that the measured $Fe(II)_{t=0}$ concentration actually exceeded the independently measured dissolved Fe concentration (Fig. 3). While unexpected, these discrepancies probably reflect small uncertainties in calibration of the Fe(II) method at high Fe(II) concentrations, where the calibration becomes nonlinear (Vedamati et al. 2014; Bolster et al. 2018).

In a one-dimensional, eddy diffusion-dominated system where the dominant source of Fe is the sediment–water interface, we would expect Fe to decrease exponentially moving away from the seafloor. Instead, these profiles do not depict a smooth exponential decay for Fe(II) or dissolved Fe at either station. We attribute the discontinuities in these profiles to wave motions and to cross-shelf advection, which would introduce Fe released nearby on the shelf to our sampling site.

The Fe(II) profiles presented in Fig. 3 are the first profiles of Fe(II) within 1 m of the seafloor on the Oregon shelf. The first study with this syringe sampler reported total Fe, as well as other parameters such as manganese, phosphate, ammonia, carbon, arsenic, mercury species, and volatilizable sulfur compounds from a 7-m-deep station in a bay and a 6-m-deep station in a lagoon (Knoery et al. 2019). Profiles from these locations had micromolar concentrations of trace metals and smooth profiles, likely because the vertical flux was far higher than any horizontal advective fluxes in these locations. We observed 20 nM Fe(II) near the seafloor at the Columbia River depocenter; however, this Fe(II) quickly decreased within 1 m of the seafloor (Fig. 3). This loss of Fe(II) likely occurred due to oxidation, as O_2 concentrations in the bottom waters of the Columbia River depocenter were approximately twice that of Heceta Bank, where this rapid Fe(II) attenuation was not predicted. Comparing the measured Fe(II) vs. O_2 concentrations for our samples reveals that Fe(II) does not significantly accumulate in samples above 75 μM O_2 and the distance from the seafloor acts as a primary control on Fe(II), since the seafloor is the primary source of Fe(II) to this region. The 75 μM O_2 threshold is consistent with the 60–80 μM O_2 threshold determined by Severmann et al. (2010) for benthic Fe fluxes. This suggests that the magnitude of benthic fluxes and accumulation of Fe(II) in the overlying waters are closely related. We found that elevated Fe(II) concentrations occur only at stations with greater than 40% mud content (Fig. 1). That trend is consistent with previous research suggesting that sediments containing mud in the region have higher levels of reactive Fe, that is presumably easy to reduce and remobilize (Roy et al. 2013).

A benthic boundary layer sampler with a different design, holding five bottles spaced every 60 cm, was deployed at a 30 m deep site in the Baltic Sea (Plass et al. 2022). They reported commonly measured first row transition metals in nanomolar concentrations, closer to those observed in our deployments. Their data generally show a linear decrease in metal concentrations away from the sediment–water interface. Their sampling interval is much larger, and they may not capture the fine structure near the seafloor that we observed. Comparing these results indicates that the magnitude of benthic flux, cross-shelf advection, and sampling resolution all influence the results of these near-bed profiles.

For some of our samples, Fe(II) and dissolved Fe concentrations approached 60 nM. These high concentrations are higher than a previous study in this area (Lohan and Bruland 2008). This could reflect spatial and temporal variability, or a severe hypoxic condition in the region in 2021 documented independently by others (Ross et al. 2022). We observed the highest Fe concentrations over Heceta Bank due to the especially low O_2 present there as well as the higher sediment mud content. Since Heceta Bank is a region where the shelf widens (Chase et al. 2007), is fed by the Umpqua river (Roy et al. 2013), and acts as a semi-retentive area (Gan and Allen 2005), this location was expected to be a hotspot for Fe release and off-shelf transport. Near the seafloor of Heceta Bank, the dissolved Fe concentration was almost entirely Fe(II), suggesting an intense supply of this material to the overlying waters. On the shallow and narrower shelf at the Newport Hydrographic line, Fe concentrations were far lower and dissolved Fe concentrations dwarfed Fe(II) concentrations, suggesting that this dissolved Fe originated from elsewhere on the continental margin. Near the Columbia River depocenter, the dissolved Fe was higher than that observed on the Newport Hydrographic Line but less than that of Heceta Bank. This observation fits with the intermediate width shelf at the Columbia River outflow.

Discussion

Controls on iron(II) concentration

Recent observations of deep Fe plumes in all three ocean ODZs (Thi Dieu Vu and Sohrin 2013; Resing et al. 2015; Bolster et al. 2022; Chinni and Singh 2022) as well as recent investigations into the mechanisms of off-shelf Fe transport (Homoky et al. 2021; König et al. 2021) have prompted interest in the conditions that enhance off-shelf Fe transport. Previous research has determined the importance of the benthic carbon oxidation rate (Elrod et al. 2004) as well as bottom water oxygen concentrations (Severmann et al. 2010) on influencing benthic Fe fluxes (Dale et al. 2015). A primary finding is that bottom water oxygen concentrations of 60–80 μM O_2 are required for benthic Fe fluxes to be observable with benthic chamber methods (Homoky et al. 2016) possibly because of rapid Fe(II) re-oxidation and removal on sinking particles (Aller et al. 2023). Water column measurements overlying the seafloor are important to assess the net accumulation of Fe in the water column.

The results presented in Figs. 2–4 demonstrate that elevated Fe(II) concentrations were only observed in samples with low O_2 concentrations, which is expected because oxidation by O_2 serves as the primary sink for Fe(II). Most of the high Fe(II) samples were collected within 30 m of the seafloor. Two samples collected at station 22 are an exception. These samples had 38–39 nM Fe(II) and were collected in a submarine canyon 70 m above the seafloor, suggesting that lateral advection from adjacent canyon walls elevated the Fe(II) concentration, rather than the underlying sediments. The results summarized in Fig. 4a indicate an O_2 threshold for Fe(II) water column concentrations around 75 μM O_2 which falls within

the range of 60–80 μM proposed by Severmann et al. (2010) as a threshold for high benthic fluxes. Our finding supports the assumption that bottom water oxygen is a major driver of Fe accumulation in bottom waters, as used in previous models of the region (Deutsch et al. 2021) and globally (Dale et al. 2015).

We can invoke the 75 μM O_2 threshold to explain the differences in Fe distribution between staions 20 and 33. At station 33, the water column within the benthic boundary layer had approximately 31 μM O_2 and O_2 concentrations were below 60 μM until 30 m above bottom (Fig. 2). These low concentrations permitted the deepest bottle samples at station 33 to retain approximately 40 nM of Fe(II) and dissolved Fe, whereas at station 20, Fe(II) concentrations were less than 5 nM in the deep bottles samples while dissolved Fe was 20 nM. Notably, station 20 exceeded the 75 μM O_2 threshold for Fe(II) accumulation within 2 m from the seafloor. These results suggest that while Fe(II) is certainly being released from the seafloor across the Oregon continental shelf, when the O_2 is above 75 μM, Fe trapping occurs, which converts Fe(II) to Fe(III) and limits dissolved Fe accumulation.

Interestingly, some of the lowest oxygen concentrations in Fig. 4a (less than 20 μM) are also associated with low Fe concentrations. These data were taken from samples overlying the continental slope and are associated with the North Pacific Oxygen Minimum Zone. Presumably Fe(II) is low because Fe supply from slope sediments is also low relative to the margins.

Analysis of sediment on the Heceta Bank, a particularly wide section of shelf that retains material from the Umpqua River, revealed an extremely high correlation between reactive iron minerals and the percent of sediment organic matter (Roy et al. 2013). Reactive iron, as defined in their protocols, is likely a source of Fe(II) to the water column under reducing conditions. We were eager to determine the relationship between sediment organic matter and Fe(II) in our study site. Since the dataset presented in Roy et al. (2013) was limited to a specific region of the shelf near the mouth of the Umpqua River including areas on the Heceta Bank, we used the usSEABED dataset and it's percent mud parameter to cover our sampling area. Comparison with Fe(II) reveals that Fe(II) only accumulated to concentrations greater than 5 nM at locations where the sediment mud content exceeds 40% (Fig. 4b). The combined datasets in Fig. 4 indicate that sediment mud content can be used to inform where Fe(II) accumulation may be expected, but bottom water O_2 is required to determine if Fe(II) will actually accumulate and persist. Note that the relationship in Fig. 4b might be due to the abundance of reactive iron in sediments with a high mud content or it could be due to other codependent factors such as the width of the continental shelf that impacts mixing and residence time.

Off-shelf iron transport

The absence of O_2 in ODZs enables Fe(II) to persist far longer than it does in a hypoxic region. In the ETSP ODZ, the half-life of Fe(II) has been estimated to be 200–2900 h (Croot et al. 2019). Since the Oregon continental shelf has waters that are usually oxic to hypoxic, residence times of Fe(II) will be far shorter, limiting the transport of Fe(II) as well as dissolved Fe in general. To evaluate the persistence of Fe(II) across the Oregon continental margin, we calculated the predicted half-lives of Fe(II) oxidation by O_2 for each Fe(II) sample. These half-lives reflect only the rate of Fe(II) oxidation, rather than its net loss, because near-shelf samples may have significant Fe(II) fluxes and high turnover.

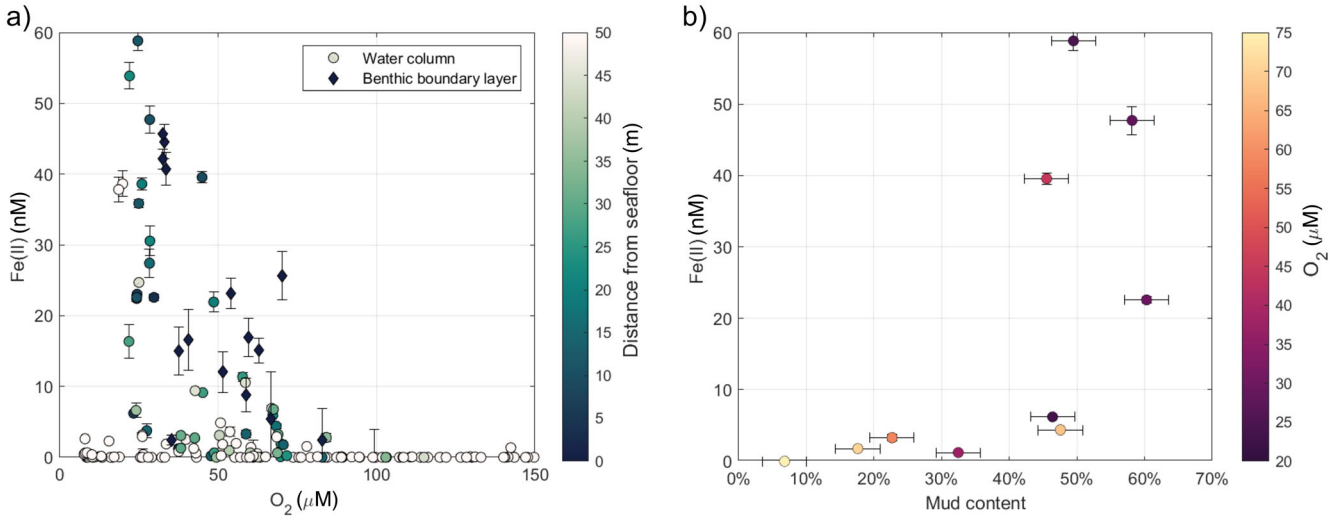

Fig. 4. (**a**) Scatter plot of O_2 and Fe(II) measured across the continental margin, with the colorbar highlighting the depth from the seafloor. Round points indicate the sample was collected from the water column with the trace metal clean rosette, whereas diamonds indicate that the sample came from a benthic lander (replotted from Fig. 3). (**b**) Scatter plot of the sediment mud content at each station vs. the deepest Fe(II) sample collected at that station, with the colorbar highlighting the deepest O_2 concentration.

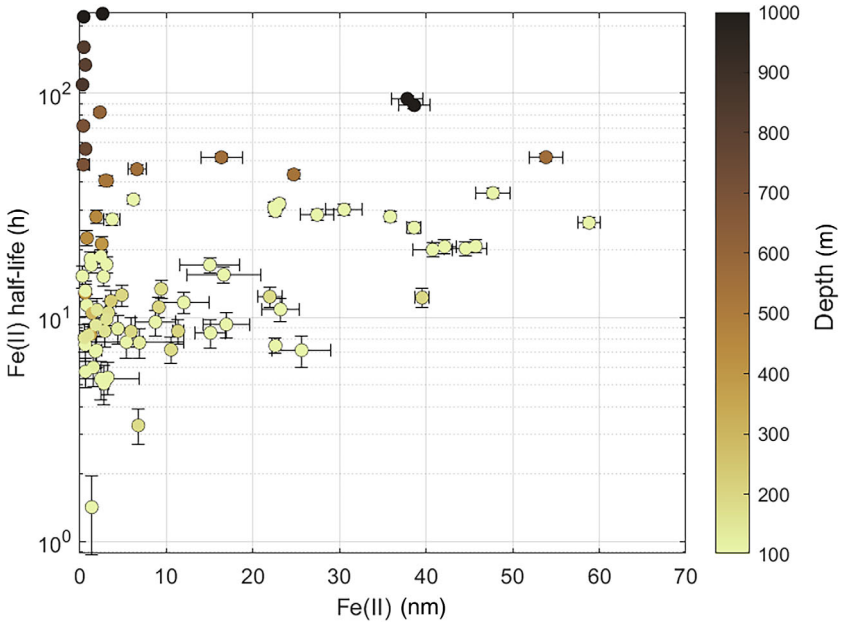

Fig. 5. Scatter plot of Fe(II) concentrations compared to their half-lives. Sample color reflects the depth where that sample was collected, whereas error bars consist of the uncertainty in Fe(II) measurements and half-lives, appropriately.

Samples with the highest Fe(II) concentrations have half-lives greater than 20 h (Fig. 5). Interestingly, samples collected deeper than 600 m tend to have significantly longer half-lives, despite their low Fe(II) concentrations. Oxidation rates at these depths are influenced by the North Pacific oxygen minimum zone, where the low O_2 concentrations, pH, and temperature all stabilize Fe(II). Fe(II) samples collected within the Oregon oxygen minimum zone had half-lives ranging from 56 to 220 h, with O_2 concentrations of 8–15 μM. The long half-lives of Fe(II) in these deep waters suggests Fe(II) may persist westward of the deep continental margin off Oregon, although that is not supported by our current data.

Deep Fe plumes are reported off several continental margins with ODZs (Saito et al. 2013; Thi Dieu Vu and Sohrin 2013; Resing et al. 2015; Moffett and German 2020). For deep Fe plumes to form, Fe has to be transported off-shelf first. In Pacific ODZs, Fe is transported off-shelf via Fe(II) export in thin layers of water that intersect the continental margin. This phenomenon is centered at 26.4 kg m^{-3} in the ETSP (Cutter et al. 2018) and 26.5 kg m^{-3} in the ETNP (Bolster et al. 2022). After leaving the shelf, Fe(II) appears to support deep plume formation as it is transported to depth via particles (Lam et al. 2020). Our data reveal Fe(II) distribution across the Oregon continental shelf for comparison with Fe(II) plumes generated within ODZs of other eastern boundary systems.

Stas. 31–33 provide an excellent opportunity to study cross-shelf transport because the Heceta Bank region is a hot spot for cross-shelf transport, revealed in an iron ROMS model applied to the region (Damien et al. 2023). In contrast to Fe(II) observations off ODZs (Vedamati et al. 2014; Bolster et al. 2022), we did not observe evidence of Fe(II) being transported off-shelf in waters that intersect with the continental shelf, between 26.5 and 26.6 kg m^{-3} (Fig. 6). We have two possible explanations for the lack of an Fe(II) plume within this density horizon. First, the O_2 concentrations within these off-shelf waters were high enough that Fe(II) oxidized to Fe(III) before it could be advected offshore. If this were the case, we might still expect a plume of dissolved Fe to be present some distance offshore before removal by scavenging. Nevertheless, there is no dissolved Fe plume at this density horizon. We did observe Fe(II) and dissolved Fe maxima at densities at the much deeper 26.8 kg m^{-3} isopycnal (Fig. 6). The maxima are deeper than expected because the isopycnal does not shoal onto Heceta Bank. There are several potential explanations for the presence of Fe(II) at this depth. A high-resolution model of dissolved Fe on the Washington coast depicts an off-shelf plume of dissolved Fe centered at 26.8 kg m^{-3} (Siedlecki et al. 2012), similar to Fig. 6, consisting of material detached from the benthic boundary layer during a downwelling event. We sampled at this location during a relaxation from upwelling, rather than intense downwelling (Supporting Information Fig. S4), so this mechanism likely did not cause the Fe(II)/dissolved Fe feature. Nevertheless, previous analysis of hypoxia on the Oregon shelf found that the period of relaxation after upwelling leads to the strongest deoxygenation (Galán et al. 2020), and this may contribute to the elevated Fe concentrations. The second explanation is that the strong undercurrent swept Fe(II) from sediments southeast of our stations and transported it to the northwest as

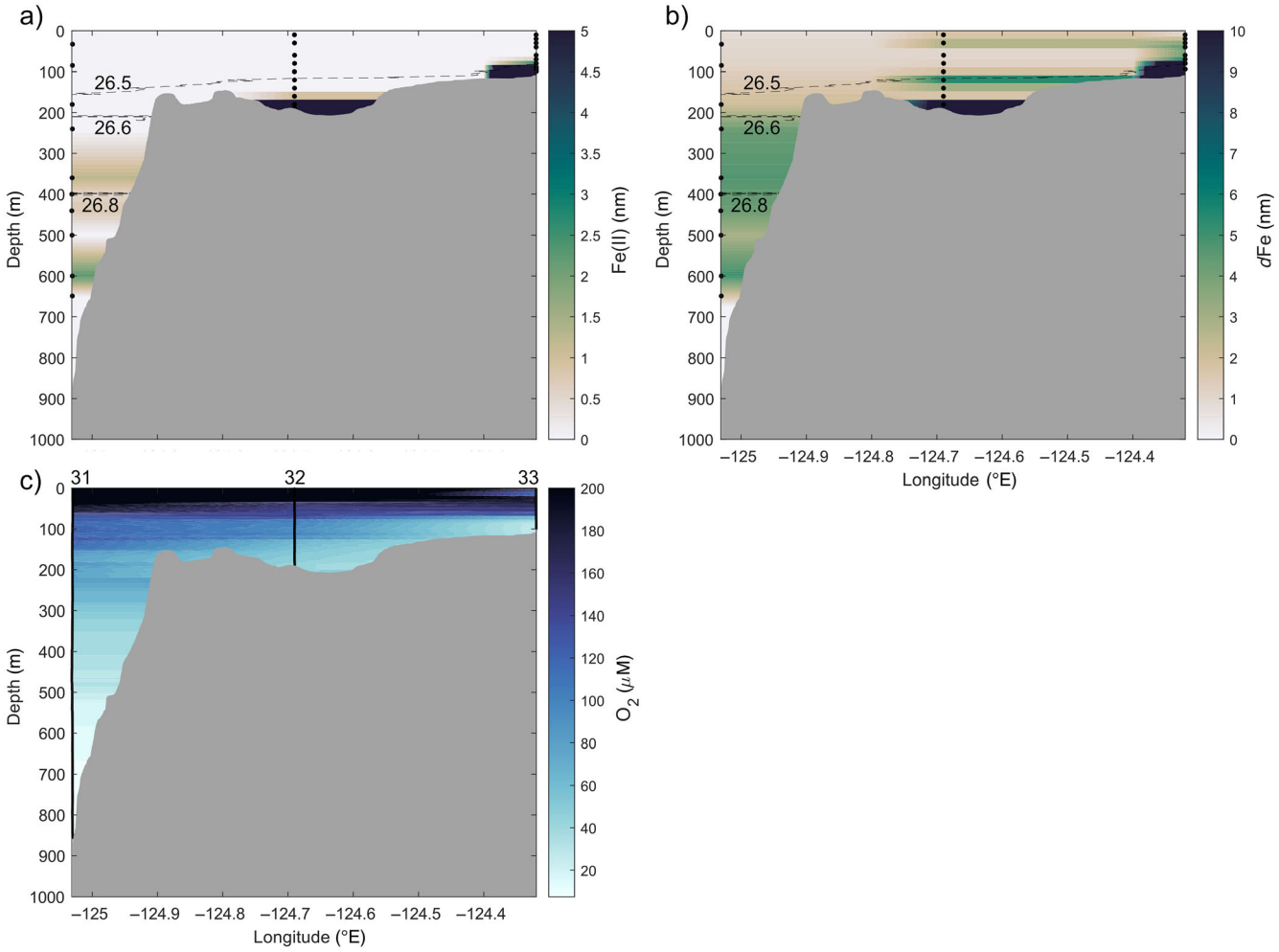

Fig. 6. Sections of (**a**) Fe(II), (**b**) dissolved Fe, and (**c**) O_2 on the Heceta Bank. These sections consist of stations 31–33, where stations 32 and 33 repeat Umpqua River-influenced stations from Severmann et al. (2010). Stations 32–33 have Fe(II) concentrations far higher than the color bar maximum, as seen in Fig. 2, but the color bar range was chosen to visualize the lower off-shelf Fe(II) concentrations. Labeled contour lines represent the potential density.

observed previously by Barth et al. (2005). We verified that the 26.8 kg m^{-3} Fe(II) feature originated from the southwest by identifying northwesterly currents at that depth using the ship-board Acoustic Doppler Current Profiler (ADCP) (Supporting Information Fig. S5). This mechanism is likely because south of Heceta Bank the seafloor deepens with a small, approximately 400 m deep shoulder, similar to the depth of the 26.8 kg m^{-3} Fe(II) feature (Supporting Information Fig. S6). There is no shallow (100–200 m) shelf in this source region, which accounts for the absence of Fe(II) within the 26.5–26.6 kg m^{-3} density range. To cross-check that this shelf shoulder could be a plausible source of Fe(II) to our sampling site, we calculated the Fe(II) concentration that would have accumulated in the shelf shoulder bottom water. Using the ADCP measured velocities, we estimated the trajectory a water parcel would have taken from the nearest shelf shoulder bottom water (approximately 20°), approximated that distance as 16.3 km, and determined the velocity to be about 0.14 m s^{-1}. We then calculated the approximate Fe(II) at that location using the same approach as $Fe(II)_{t=0}$, using the measured Fe(II) concentration, O_2 concentration, pH, and the 31.5 h advection time. This calculation reveals that bottom waters on the shelf shoulder would need to contain approximately 3 nM Fe(II) for the observed Fe(II) concentration off Heceta Bank at 26.8 kg m^{-3}. This is a reasonable concentration based on our data elsewhere.

We attribute the Fe(II) and dissolved Fe features at 600 m to Fe(II) released from the continental slope and stabilized by the North Pacific oxygen minimum zone. At these stations, Fe(II) was sampled off the CTD rosette to acquire samples near the seafloor, whereas dissolved Fe was only sampled off the trace metal clean rosette. It is important to note that the iron distributions we observed across Heceta Bank may be more pronounced than those that exist more generally across

hypoxic Eastern Boundary Upwelling Systems. Heceta Bank is a particularly large topographical feature, so it retains river-deposited organic matter and experiences elevated amounts of remineralization (Siedlecki et al. 2015) as well as being a semi-retentive region (Gan and Allen 2005). These factors facilitate oxygen depletion, Fe accumulation, and induce off-shelf transport events linked to the California Undercurrent. Nevertheless, these results indicate that off-shelf iron transport from shelf regions with seasonal hypoxia such as Oregon differ significantly from shelf systems within ODZs that are permanently anaerobic.

Our data provide a high-resolution description of iron accumulation and redox speciation in near-bottom waters on the Oregon continental margin during summer. The seasonal hypoxia observed in this region causes it to be a particularly significant source of iron to nearby highly productive and often iron-limited ecosystems. The potential emergence of seasonal anoxia within these waters also suggests that this region could become a far larger source of iron to the North Pacific in the future. We analyzed our data within the context of many previously established relationships with iron, such as bottom water O_2, shelf width, and sediment organic carbon to improve our mechanistic understanding of iron released from continental reducing margins.

Hypoxia is increasing in strength and duration on the Oregon continental shelf (Pierce et al. 2012), and intermediate waters of the North Pacific are also experiencing deoxygenation (Whitney et al. 2007). Lower O_2 will lead to elevated Fe(II) release and persistence in the water column, increasing the role of the Oregon continental margin as an Fe source. A Japanese survey within the international GEOTRACES program provided strong evidence for the formation of subsurface plumes off the Oregon coast (Wong et al. 2022), and our work suggests that hypoxia on the Oregon shelf and slope can influence basin-scale biogeochemistry. Understanding and simulating continental margin Fe supply will provide helpful information for predicting the condition of the future coastal ocean. Intensive modeling and monitoring already occurs for these waters due to their economic significance (Lubchenco et al. 2019), and an improved understanding of Fe, a critical nutrient in this region, will advance these efforts.

Data availability statement

All data and code used in this paper can be found at https://github.com/NatalyaEvans/Oregon_Fe2. We analyze several other data products in this paper, and we include them in this repository as well. Data are also stored in the Biological and Chemical Data Management Office (Moffett 2023).

References

Adams, K. A., J. A. Barth, and R. K. Shearman. 2016. Intraseasonal cross-shelf variability of hypoxia along the Newport, Oregon, hydrographic line. J. Phys. Oceanogr. **46**: 2219–2238. doi:10.1175/JPO-D-15-0119.1

Aller, R. C., I. P. Dwyer, D. S. Perger, C. Heilbrun, N. Volkenborn, and L. M. Wehrmann. 2023. Estimating benthic Fe and reactive solute fluxes. Mar. Chem. **249**: 104221.

Barth, J. A., S. D. Pierce, and R. M. Castelao. 2005. Time-dependent, wind-driven flow over a shallow midshelf submarine bank. J. Geophys. Res. Oceans **110**. doi:10.1029/2004JC002761

Berger, C. J., S. M. Lippiatt, M. G. Lawrence, and K. W. Bruland. 2008. Application of a chemical leach technique for estimating labile particulate aluminum, iron, and manganese in the Columbia River plume and coastal waters off Oregon and Washington. J. Geophys. Res. Oceans **113**. doi:10.1029/2007JC004703

Biguri, A. 2021. Perceptually uniform colormaps. MATLAB Central File Exchange. https://www.mathworks.com/matlabcentral/fileexchange/51986-perceptually-uniform-colormaps

Bolster, K. M., M. I. Heller, M. R. Mulholland, and J. W. Moffett. 2022. Iron and manganese accumulation within the eastern tropical North Pacific oxygen deficient zone. Geochim. Cosmochim. Acta **334**: 259–272. doi:10.1016/j.gca.2022.07.013

Bolster, K. M., M. I. Heller, and J. W. Moffett. 2018. Determination of iron(II) by chemiluminescence using masking ligands to distinguish interferences. Limnol. Oceanogr. Methods **16**: 750–759. doi:10.1002/lom3.10279

Boyd, P. W. and M. J. Ellwood. 2010. The biogeochemical cycle of iron in the ocean. Nat. Geosci. **3**: 675–682.

Bruland, K. W., M. C. Lohan, A. M. Aguilar-Islas, G. J. Smith, B. Sohst, and A. Baptista. 2008. Factors influencing the chemistry of the near-field Columbia River plume: Nitrate, silicic acid, dissolved Fe, and dissolved Mn. Journal of Geophysical Research: Oceans **113**. doi:10.1029/2007JC004702

Buck, K. N., M. C. Lohan, C. J. Berger, and K. W. Bruland. 2007. Dissolved iron speciation in two distinct river plumes and an estuary: Implications for riverine iron supply. Limnol. Oceanogr. **52**: 843–855.

Canfield, D. E., T. W. Lyons, and R. Raiswell. 1996. A model for iron deposition to euxinic Black Sea sediments. Am. J. Sci. **296**: 818–834. doi:10.2475/ajs.296.7.818

Chan, F., J. Barth, K. Kroeker, J. Lubchenco, and B. Menge. 2019. The dynamics and impact of ocean acidification and hypoxia: Insights from sustained investigations in the Northern California current large marine ecosystem. Oceanography **32**: 62–71. doi:10.5670/oceanog.2019.312

Chan, F., J. A. Barth, J. Lubchenco, A. Kirincich, H. Weeks, W. T. Peterson, and B. A. Menge. 2008. Emergence of anoxia in the California current large marine ecosystem. Science **319**: 920. doi:10.1126/science.1149016

Chase, Z., P. G. Strutton, and B. Hales. 2007. Iron links river runoff and shelf width to phytoplankton biomass along

the U.S. West Coast. Geophys. Res. Lett. **34**. doi:10.1029/2006GL028069

Chinni, V., and S. K. Singh. 2022. Dissolved iron cycling in the Arabian Sea and sub-tropical gyre region of the Indian Ocean. Geochim. Cosmochim. Acta **317**: 325–348.

Croot, P. L., M. I. Heller, and K. Wuttig. 2019. Redox processes impacting the flux of iron(II) from shelf sediments to the OMZ along the Peruvian shelf. ACS Earth Space Chem. **3**: 537–549. doi:10.1021/acsearthspacechem.8b00203

Cutter, G. A., J. W. Moffett, M. C. Nielsdóttir, and V. Sanial. 2018. Multiple oxidation state trace elements in suboxic waters off Peru: In situ redox processes and advective/diffusive horizontal transport. Mar. Chem. **201**: 77–89. doi:10.1016/j.marchem.2018.01.003

Dale, A. W., L. Nickelsen, F. Scholz, C. Hensen, A. Oschlies, and K. Wallmann. 2015. A revised global estimate of dissolved iron fluxes from marine sediments. Global Biogeochem. Cycles **29**: 691–707. doi:10.1002/2014GB005017

Damien, P., D. Bianchi, J. C. McWilliams, F. Kessouri, C. Deutsch, R. Chen, and L. Renault. 2023. Enhanced biogeochemical cycling along the US West Coast shelf. Global biogeochemical cycles **37**: e2022GB007572.

Deutsch, C., and others. 2021. Biogeochemical variability in the California Current system. Prog. Oceanogr. **196**: 102565.

Elrod, V. A., W. M. Berelson, K. H. Coale, and K. S. Johnson. 2004. The flux of iron from continental shelf sediments: A missing source for global budgets. Geophys. Res. Lett. **31**. doi:10.1029/2004GL020216

Evans, N., I. D. Schroeder, M. Pozo Buil, M. G. Jacox, and S. J. Bograd. 2020. Drivers of subsurface deoxygenation in the Southern California Current System. Geophys. Res. Lett. **47**: e2020GL089274. doi:10.1029/2020GL089274

Frenger, I., and others. 2018. Biogeochemical role of subsurface coherent eddies in the ocean: Tracer cannonballs, hypoxic storms, and microbial stewpots? Global Biogeochem. Cycl. **32**: 226–249.

Fuchsman, C. A., A. H. Devol, Z. Chase, C. E. Reimers, and B. Hales. 2015. Benthic fluxes on the Oregon shelf. Estuar. Coast. Shelf Sci. **163**: 156–166. doi:10.1016/j.ecss.2015.06.001

Galán, A., M. J. Zirbel, G. S. Saldías, F. Chan, and R. Letelier. 2020. The role of upwelling intermittence in the development of hypoxia and nitrogen loss over the Oregon shelf. J. Mar. Syst. **207**: 103342. doi:10.1016/j.jmarsys.2020.103342

Gan, J., and J. S. Allen. 2005. Modeling upwelling circulation off the Oregon coast. J. Geophys. Res. Oceans **110**. doi:10.1029/2004JC002692

Glover, D. M., W. J. Jenkins, and S. C. Doney. 2011. Modeling methods for marine science. Cambridge Univ. Press.

González-Santana, D., and others. 2021. Variability in iron (II) oxidation kinetics across diverse hydrothermal sites on the northern Mid Atlantic Ridge. Geochim. Cosmochim. Acta **297**: 143–157.

Hatta, M., C. I. Measures, J. Wu, S. Roshan, J. N. Fitzsimmons, P. Sedwick, and P. Morton. 2015. An overview of dissolved Fe and Mn distributions during the 2010–2011 U.S. GEOTRACES North Atlantic cruises: GEOTRACES GA03. Deep-Sea Res. II Top. Stud. Oceanogr. **116**: 117–129. doi:10.1016/j.dsr2.2014.07.005

Homoky, W. B., T. M. Conway, S. G. John, D. König, F. Deng, A. Tagliabue, and R. A. Mills. 2021. Iron colloids dominate sedimentary supply to the ocean interior. Proc. Nat. Acad. Sci. USA **118**: e201607818. doi:10.1073/pnas.2016078118

Homoky, W. B., and others. 2016. Quantifying trace element and isotope fluxes at the ocean–sediment boundary: A review. Philos. Trans. R Soc. A Math. Phys. Eng. Sci. **374**: 20160246. doi:10.1098/rsta.2016.0246

Hunter, J. D. 2007. Matplotlib: A 2D graphics environment. Comput. Sci. Eng. **9**: 90–95. doi:10.1109/MCSE.2007.55

Jackson, S. L., J. Spence, D. J. Janssen, A. R. S. Ross, and J. T. Cullen. 2018. Determination of Mn, Fe, Ni, Cu, Zn, Cd and Pb in seawater using offline extraction and triple quadrupole ICP-MS/MS. J. Anal. At. Spectrom **33**: 304–313. doi:10.1039/C7JA00237H

Jickells, T. D., and others. 2005. Global iron connections between desert dust, ocean biogeochemistry, and climate. Science **308**: 67–71. doi:10.1126/science.1105959

Johnson, K. S., F. P. Chavez, and G. E. Friederich. 1999. Continental-shelf sediment as a primary source of iron for coastal phytoplankton. Nature **398**: 697–700. doi:10.1038/19511

König, D., T. M. Conway, M. J. Ellwood, W. B. Homoky, and A. Tagliabue. 2021. Constraints on the cycling of iron isotopes from a global ocean model. Global Biogeochem. Cycles **35**: e2021GB006968. doi:10.1029/2021GB006968

Knoery, J., D. Cossa, B. Thomas, G. Gregory, and S. Rigaud. 2019. Susane, a device for sampling chemical gradients in the benthic water column. Limnol. Oceanogr. Methods **17**: 331–342. doi:10.1002/lom3.10317

Kulm, L. D., R. C. Roush, J. C. Harlett, R. H. Neudeck, D. M. Chambers, and E. J. Runge. 1975. Oregon continental shelf sedimentation: Interrelationships of facies distribution and sedimentary processes. J. Geol. **83**: 145–175.

Lam, P. J., and J. K. Bishop. 2008. The continental margin is a key source of iron to the HNLC North Pacific Ocean. Geophysical Research Letters **35**: 1–5.

Lam, P. J., M. I. Heller, P. E. Lerner, J. W. Moffett, and K. N. Buck. 2020. Unexpected source and transport of iron from the deep Peru margin. ACS Earth Space Chem. **4**: 977–992. doi:10.1021/acsearthspacechem.0c00066

Lohan, M. C., and K. W. Bruland. 2008. Elevated Fe(II) and dissolved Fe in hypoxic shelf waters off Oregon and Washington: An enhanced source of iron to coastal upwelling regimes. Environ. Sci. Technol. **42**: 6462–6468. doi:10.1021/es800144j

Lubchenco, J., and S. D. Gaines. 2019. A new narrative for the ocean. Science **364**: 911–911.D.

McDougall, T. J., and P. M. Barker. 2011. Getting started with TEOS-10 and the Gibbs seawater (GSW) oceanographic toolbox, SCOR/IAPSO WG127, **127**: 1–28.

Meinvielle, M., and G. C. Johnson. 2013. Decadal water-property trends in the California undercurrent, with implications for ocean acidification. J. Geophys. Res. Oceans **118**: 6687–6703. doi:10.1002/2013JC009299

Milne, A., W. Landing, M. Bizimis, and P. Morton. 2010. Determination of Mn, Fe, Co, Ni, Cu, Zn, Cd and Pb in seawater using high resolution magnetic sector inductively coupled mass spectrometry (HR-ICP-MS). Anal. Chim. Acta **665**: 200–207. doi:10.1016/j.aca.2010.03.027

Moffett, J. W. 2023. Benthic iron data on the Oregon shelf from samples collected on R/V Oceanus cruise OC2107A during July to Sugust 2021. Biological and Chemical Oceanography Data Management Office (BCO-DMO). (Version 1) Version Date 2023-04-26. http://lod.bco-dmo.org/id/dataset/894761

Moffett, J. W., and C. R. German. 2020. Distribution of iron in the Western Indian Ocean and the Eastern tropical South pacific: An inter-basin comparison. Chem. Geol. **532**: 119334.

Molemaker, M. J., J. C. McWilliams, and W. K. Dewar. 2015. Submesoscale instability and generation of mesoscale anticyclones near a separation of the California undercurrent. Journal of Physical Oceanography **45**: 613–629.

Moore, C. M., and others. (2013). Processes and patterns of oceanic nutrient limitation. Nat. Geosci. **6**: 701–710. doi:10.1038/ngeo1765

Nittrouer, C. A., R. W. Sternberg, R. Carpenter, and J. T. Bennett. 1979. The use of Pb-210 geochronology as a sedimentological tool: Application to the Washington continental shelf. Mar. Geol. **31**: 297–316. doi:10.1016/0025-3227(79)90039-2

Noble, A. E., and others. 2012. Basin-scale inputs of cobalt, iron, and manganese from the Benguela-Angola front to the South Atlantic Ocean. Limnol. Oceanogr. **57**: 989–1010. doi:10.4319/lo.2012.57.4.0989

Pierce, S. D., J. A. Barth, R. K. Shearman, and A. Y. Erofeev. 2012. Declining oxygen in the Northeast Pacific*. J. Phys. Oceanogr. **42**: 495–501. doi:10.1175/JPO-D-11-0170.1

Plass, A., A.-K. Retschko, M. Türk, T. Fischer, and F. Scholz. 2022. A novel device for trace metal-clean sampling of bottom water and suspended particles at the ocean's lower boundary: The Benthic Trace Profiler. Limnol. Oceanogr. Methods **20**: 102–114. doi:10.1002/lom3.10473

Python Software Foundation. 2022. Python language reference, 3.7.13 documentation. https://docs.python.org/release/3.7.13/

Raiswell, R., and D. E. Canfield. 2012. Section 4. Iron transport by the shelf-to-basin shuttle. Geochemical Perspectives **1**: 42–55.

Rapp, I., C. Schlosser, D. Rusiecka, M. Gledhill, and E. P. Achterberg. 2017. Automated preconcentration of Fe, Zn, Cu, Ni, Cd, Pb, Co, and Mn in seawater with analysis using high-resolution sector field inductively-coupled plasma mass spectrometry. Anal. Chim. Acta **976**: 1–13. doi:10.1016/j.aca.2017.05.008

Raybaut, P. 2009. Spyder 5.1.5 documentation. https://www.spyder-ide.org/

Reed, D. C., B. G. Gustafsson, and C. P. Slomp. 2016. Shelf-to-basin iron shuttling enhances vivianite formation in deep Baltic Sea sediments. Earth Planet. Sci. Lett. **434**: 241–251. doi:10.1016/j.epsl.2015.11.033

Resing, J. A., P. N. Sedwick, C. R. German, W. J. Jenkins, J. W. Moffett, B. M. Sohst, and A. Tagliabue. 2015. Basin-scale transport of hydrothermal dissolved metals across the South Pacific Ocean. Nature **523**: 200–203. doi:10.1038/nature14577

Ross, T., and others. 2022. Northeast Pacific update: Summer 2021 low oxygen event on the west coast of North America. PICES Press **30**: 38–42.

Roy, M., and others. 2013. Reactive iron and manganese distributions in seabed sediments near small mountainous rivers off Oregon and California (USA). Cont. Shelf Res. **54**: 67–79. doi:10.1016/j.csr.2012.12.012

Saito, M. A., A. E. Noble, A. Tagliabue, T. J. Goepfert, C. H. Lamborg, and W. J. Jenkins. 2013. Slow-spreading submarine ridges in the South Atlantic as a significant oceanic iron source. Nat. Geosci. **6**: 775–779.

Santana-Casiano, J. M., M. González-Dávila, and F. J. Millero. 2005. Oxidation of nanomolar levels of Fe(II) with oxygen in natural waters. Environ. Sci. Technol. **39**: 2073–2079. doi:10.1021/es049748y

Severmann, S., J. McManus, W. M. Berelson, and D. E. Hammond. 2010. The continental shelf benthic iron flux and its isotope composition. Geochim. Cosmochim. Acta **74**: 3984–4004. doi:10.1016/j.gca.2010.04.022

Siedlecki, S. A., A. Mahadevan, and D. E. Archer. 2012. Mechanism for export of sediment-derived iron in an upwelling regime. Geophys. Res. Lett. **39**. doi:10.1029/2011GL050366

Siedlecki, S. A., N. S. Banas, K. A. Davis, S. Giddings, B. M. Hickey, P. MacCready, T. Connolly, and S. Geier. 2015. Seasonal and interannual oxygen variability on the Washington and Oregon continental shelves. J. Geophys. Res. Oceans **120**: 608–633. doi:10.1002/2014JC010254

Tagliabue, A., A. R. Bowie, P. W. Boyd, K. N. Buck, K. S. Johnson, and M. A. Saito. 2017. The integral role of iron in ocean biogeochemistry. Nature **543**: 51–59.

The MathWorks, Inc. 2018. MATLAB release 2018b.

Thi Dieu Vu, H., and Y. Sohrin. 2013. Diverse stoichiometry of dissolved trace metals in the Indian Ocean. Sci. Rep. **3**: 1745. doi:10.1038/srep01745

Thomson, R. E., and M. V. Krassovski. 2010. Poleward reach of the California undercurrent extension. J. Geophys. Res. Oceans **115**. doi:10.1029/2010JC006280

Thyng, K., C. Greene, R. Hetland, H. Zimmerle, and S. DiMarco. 2016. True colors of oceanography: Guidelines for effective and accurate colormap selection. Oceanography **29**: 9–13. doi:10.5670/oceanog.2016.66

Ulloa, O., D. E. Canfield, E. F. DeLong, R. M. Letelier, and F. J. Stewart. 2012. Microbial oceanography of anoxic oxygen minimum zones. Proc. Nat. Acad. Sci. USA **109**: 15996–16003. doi:10.1073/pnas.1205009109

Vedamati, J., T. Goepfert, and J. W. Moffett. 2014. Iron speciation in the eastern tropical South Pacific oxygen minimum zone off Peru. Limnol. Oceanogr. **59**: 1945–1957. doi:10.4319/lo.2014.59.6.1945

Vraspir, J. M., and A. Butler. 2009. Chemistry of marine ligands and siderophores. Ann. Rev. Mar. Sci. **1**: 43–63.

Wetz, M. S., B. Hales, Z. Chase, P. A. Wheeler, and M. M. Whitney. 2006. Riverine input of macronutrients, iron, and organic matter to the coastal ocean off Oregon, U.S.A., during the winter. Limnol. Oceanogr. **51**: 2221–2231. doi:10.4319/lo.2006.51.5.2221

Whitney, F. A., H. J. Freeland, and M. Robert. 2007. Persistently declining oxygen levels in the interior waters of the eastern subarctic Pacific. Progress in Oceanography **75**: 179–199. doi:10.1016/j.pocean.2007.08.007

Wong, K. H., J. Nishioka, T. Kim, and H. Obata. 2022. Long-range lateral transport of dissolved manganese and iron in the subarctic Pacific. Journal of Geophysical Research: Oceans **127**: e2021JC017652. doi:10.1029/2021JC017652

Acknowledgments

We acknowledge NSF OCE 2023708 for supporting this research. The development of the benthic sampler lander was supported by Oregon Sea Grant Project number: R/HBT-23-Reimers2022 with the syringe sampler (Susane) graciously provided from Ifremer. We appreciate the support provided by R/V *Oceanus* crew and marine technicians during our cruise, specifically Emily Shimada, Michael Tepper-Rasmussen, and Sabrina Taraboletti. We would also like to thank our collaborators in the Bianchi lab, specifically Daniel McCoy, Pierre Damien, and Anh Pham.

Conflict of Interest

None declared.

Submitted 12 April 2023
Revised 13 October 2023
Accepted 03 November 2023

Associate editor: Robinson W. Fulweiler